Progress In Electromagnetics Research, PIER 41, 211–235, 2003

ANALYSIS AND APPLICATIONS OF UNIPLANAR COMPACT PHOTONIC BANDGAP STRUCTURES

C. C. Chang, Y. Qian, and T. Itoh

Department of Electrical Engineering
University of California Los Angeles
405 Hilgard Ave.
Los Angeles, CA 90095, USA

Abstract—This paper reviews recent advancements in the research and development of Uniplanar Compact Photonic Bandgap (UC-PBG) structures for microwave and millimeter-wave applications. These planar periodic structures are particularly attractive and have been intensively investigated due to their easy fabrication, low cost, and compatibility with standard planar circuit technology. In this paper, basic properties of UC-PBG will be studied such as the slow-wave effect, distinct stopband and passband, leakage suppression of surface waves, and realization of a magnetic surface. Owing to the different features of UC-PBG, these structures have been applied to microwave circuits to improve microstrip filters and patch antennas, to perform harmonic tuning in power amplifiers, to suppress leakage in conductor-backed coplanar waveguide, to realize TEM waveguides, and to implement low-profile cavity-backed slot antennas.

1. INTRODUCTION

Photonic bandgap (PBG) structures are periodic structures in which optical waves are forbidden in certain frequency bands. PBG structures can be one-, two- or three-dimensional periodic structures. Due to the analogy between electromagnetic wave propagation in multidimensional periodic structures and electron wave propagation in crystals, PBG structures find applications in both the optics and microwave regime. Although one- and two-dimensional periodic structures have long been investigated in the microwave community, new concepts and ideas recently developed in the optics regime [1–2] have sparked new interest in the microwave area. Among the new ideas, the most attractive to microwave engineers is the ability to forbid electromagnetic wave propagation in either all or selected directions. Extensive investigations have been conducted to translate and apply these new concepts to the microwave and millimeter-wave domain [3–5] and several applications at microwave frequencies have been developed, including antenna substrates [6–8], resonant cavities, and filters [9].

Electromagnetic crystals at microwave frequencies can be realized by scaling the structures used at optical frequencies. For example, by micromachining holes in dielectric slabs, a two-dimensional periodic variation of the material refractive dielectric is achieved [10]. Machined slabs can also be stacked to create a three-dimensional periodic variation of the refractive index [11].

Many attempts to reduce the physical size of these periodic structures have been reported in the literature. One such method is to use metallo-dielectric structures [12–14]. The basic idea here is the introduction of a periodic network of LC-elements to shorten the wavelength of the propagating wave. An effective example of metallo-dielectric crystals is given by the high-impedance ground plane described in [15], which is employed to improve patch antenna performance in [16]. It is comprised of a grounded dielectric slab periodically loaded with a square lattice of square metallic pads. The edges of the pads are a few mils apart, realizing a 2D periodic network

of capacitors. Each pad is connected to ground through one via at its center, which provides the inductive part of the LC-network.

The above approach, although very effective, requires a non-planar fabrication process. Recent research efforts at the authors' group focus on the development of planar electromagnetic crystals that do not need vias and that can be easily integrated in microwave and millimeter-wave circuits. The structure consists of compact crystals periodically distributed in two dimensions, henceforth referred to as Uniplanar Compact PBG (UC-PBG), which realizes a 2D periodic network of LC circuits without introducing vias.

2. UNIPLANAR COMPACT PHOTONIC BANDGAP STRUCTURE

The UC-PBG structure consists of a uniformly distributed periodic metallic pattern on one side of a dielectric slab. It exhibits some interesting features such as distinctive passband and stopband, slow-wave effects, low attenuation in the passband, and suppression of surface waves when serving as the ground plane of planar microstrip circuits. Moreover, the UC-PBG structure can also be used to realize a perfectly magnetic conducting (PMC) surface, which finds applications in designing a TEM waveguide and a low profile cavity backed slot antenna.

2.1. Microstrip-Guided Waves in UC-PBG Structure

Fig. 1 shows the schematic of the UC-PBG structure and corresponding geometric parameters. This periodic pattern serves as the ground plane in a microstrip-line structure. Each lattice (Fig. 1(b)) is connected to its four adjacent neighbors via narrow strips. Each of these strips has an inset to increase the inductance per unit length (L) of the microstrip line. Additionally, the gaps between adjacent lattices create a coupling capacitance, increasing the capacitance per unit length (C). By changing the geometry of the strips and gaps, we can change L and C, thereby controlling the slow-wave effect. This is particularly attractive since we can control the slow-wave effect without changing the substrate properties.

Fig. 2 shows a 50-microstrip line etched on an RT/Duroid 6010 substrate with a dielectric constant of 10.2 and thickness of 0.635 mm. The UC-PBG pattern is etched on the bottom side of the dielectric slab. Fig. 3 shows the Finite-Difference Time-Domain (FDTD) simulated and measured S-parameters of the microstrip line. In FDTD simulation, a distinctive stopband can be observed at frequencies above

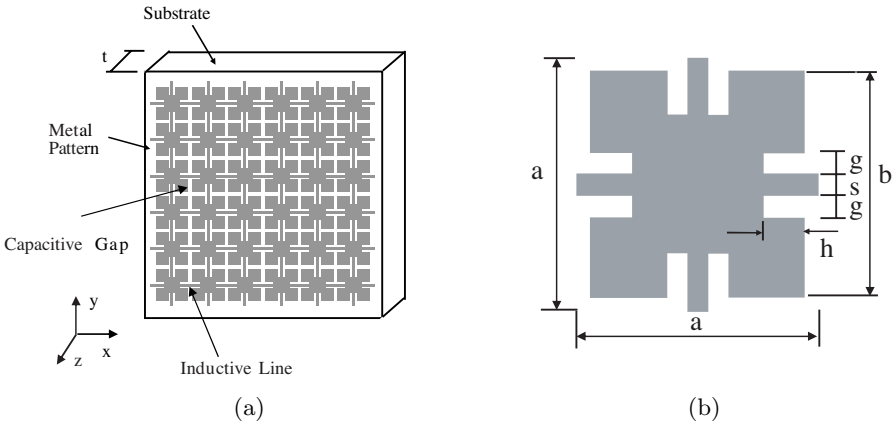

(a) (b)

Figure 1. (a) Schematic of UC-PBG metallic pattern on a dielectric slab. Slab relative dielectric constant is 10.2 and thickness is 0.635 mm. (b) Unit cell of the UC-PBG structure. Parameters: $a = 3.048$ mm; $b = 2.794$ mm; $h = 0.6985$ mm; $s = g = 0.254$ mm.

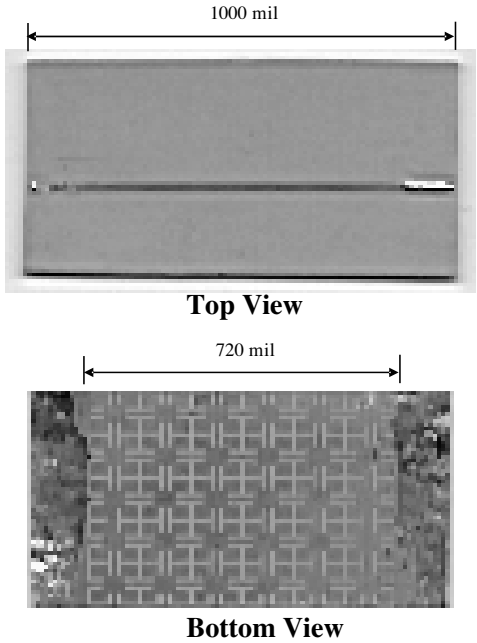

Figure 2. Photographs of top and bottom layers of the microstrip on UC-PBG ground plane.

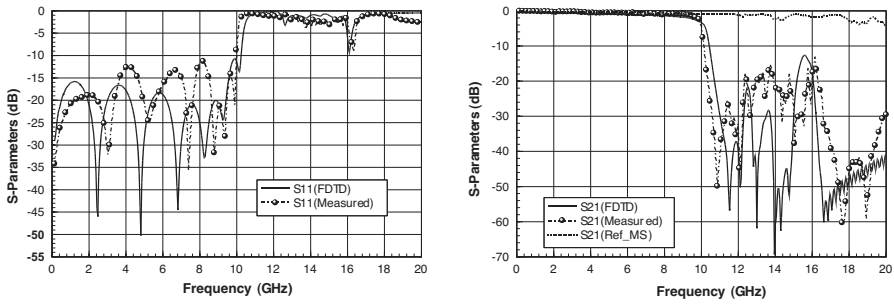

(a) (b)

Figure 3. Simulated and measured return loss of the microstrip on UC-PBG ground. (a) Return loss and (b) insertion loss.

10 GHz, where the transmission coefficient (S_{21}) is lower than -20 dB, except for a small band at $15 \sim 16$ GHz. The measured S_{21} shows -15 to -17 dB from $12 \sim 15$ GHz because of the multiple reflections from the substrate edges in the measurement. S_{21} is quite flat in the low-frequency passband and compares favorably to S_{21} for a standard 50-transmission line. In fact, the insertion loss in the passband remains flat even when an alignment offset between the microstrip line and UC-PBG lattice is present [17]. The slow-wave factor, as shown in Fig. 4, has been measured to be 1.2 to 2.4 times larger than that of a conventional microstrip line [18]. This slow-wave effect is due to the increased inductance and capacitance per unit length. Since both the inductance and capacitance per unit length increase, the impedance of the microstrip line on UC-PBG ground plane remains close to 50 below the cutoff. This is in direct contrast to other structures such metal-insulator-semiconductor (MIS) transmission lines, where the inductance/capacitance increase disproportionately, resulting in very low impedances that are difficult to match to [19].

2.2. Surface Waves in UC-PBG Structure

To investigate surface-wave propagation along the UC-PBG lattice, two dielectric slabs clad with the UC-PBG pattern are constructed — one on a conductor-backed slab and the other on a bare dielectric slab. In both cases, a stopband for surface waves propagating along the structure still appears when the condition $\beta a = \pi$, is satisfied. However, the presence of the LC-networks reduces the wavelength of the surface wave, so that the period of the UC-PBG is significantly smaller than a half-wavelength in free-space.

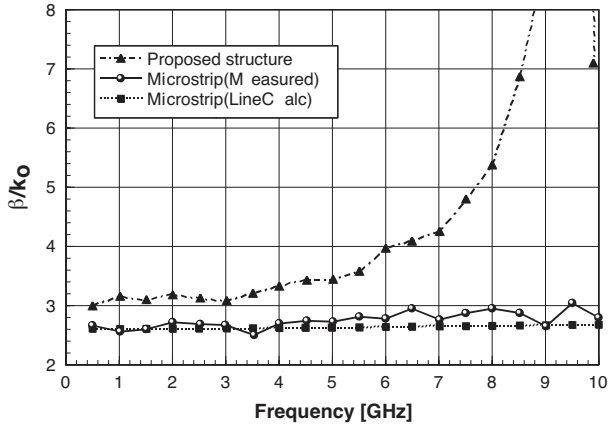

Figure 4. Slow-wave factor of a microstrip line on the UC-PBG ground plane in comparison with a conventional microstrip line.

Fig. 5 shows the dispersion diagram for the two different cases of UC-PBG used on a bare dielectric slab (Fig. 5(a)) and on a conductor-backed dielectric slab (Fig. 5(b)). Several differences can be noted between the two diagrams. First, while the UC-PBG on a bare dielectric slab presents a wide stopband between the third and fourth mode in the frequency range 16.1 to 26.1 GHz, the UC-PBG on a conductor-backed dielectric slab has two stopbands. The first stopband is between the first and second mode, spanning the frequency range 11.3 to 14.1 GHz; the second is between the third and fourth modes in the frequency range 18.9 to 23 GHz. Moreover, the second and fourth modes of the conductor-backed dielectric slab UC-PBG do not show any cut-off frequency as seen instead for the second and fourth modes of the bare dielectric slab UC-PBG.

The fundamental mode of both structures is a TM-like mode with a strong longitudinal component of the electric field. Computations show that, as expected, the effective dielectric constant of the fundamental mode is higher in the case of the conductor-backed dielectric slab UC-PBG. This is due to the fact that the backed conductor confines the electric field inside the high permittivity region. The second and third modes for both cases are predominantly TE modes with a strong transverse component of the electric field. Fig. 6 shows the electric (white arrow) and magnetic (black arrow) fields, as well as the normalized electric energy distribution (colors) for the first and second modes at X point of the Brillouin zone in Fig. 5(b). Fields and energy are displayed at the plane in the substrate right underneath the

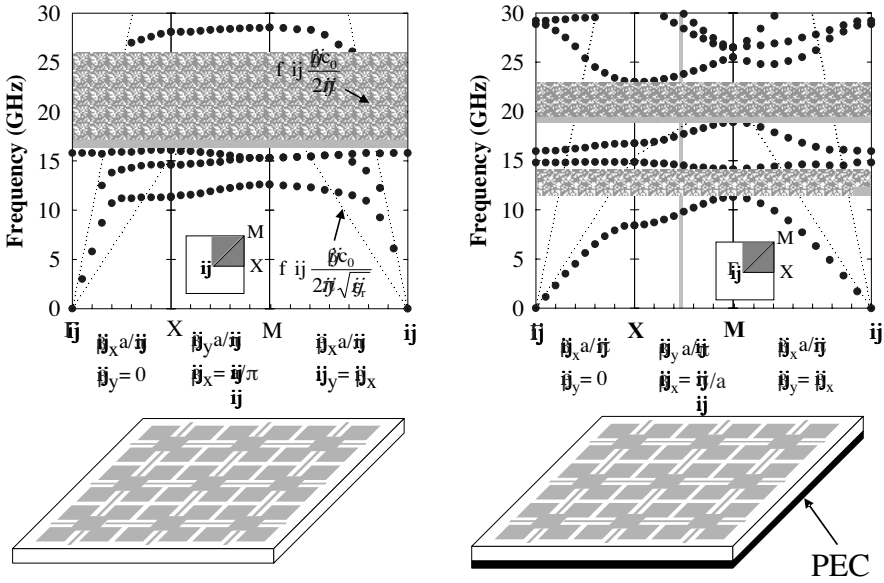

(a) (b)

Figure 5. Dispersion diagrams of UC-PBG structures patterned on (a) a bare dielectric slab and (b) a conductor-backed dielectric slab. The grey areas in both figures represent stop band.

metallic pattern.

The nature of wave propagation along the microstrip-based UC-PBG structure can be further elucidated by considering the Brillouin zone [2] of the lattice as depicted in Fig. 5. The $-X$ section describes mode propagation along the UC-PBG structure in a direction parallel to the primitive vectors ($a\hat{x}$ or $a\hat{y}$ in Fig. 1(a)) of the square lattice. The first TM-like mode has a cut-off frequency at the X point of 11.4 GHz for the case of UC-PBG on a bare dielectric slab, and 8.4 GHz for the case of UC-PBG on a conductor-backed dielectric slab. The measured cut-off frequency for the microstrip-guided mode is 10 GHz. As expected, this value is between the two extreme cases of UC-PBG on a bare and conductor-backed dielectric slab.

2.3. Plane Waves Impinge upon UC-PBG Structure

The main difference in electrical property between a perfect-electric conductor (PEC) and perfect-magnetic conductor (PMC) can be observed by measuring the reflection coefficient when the surfaces are

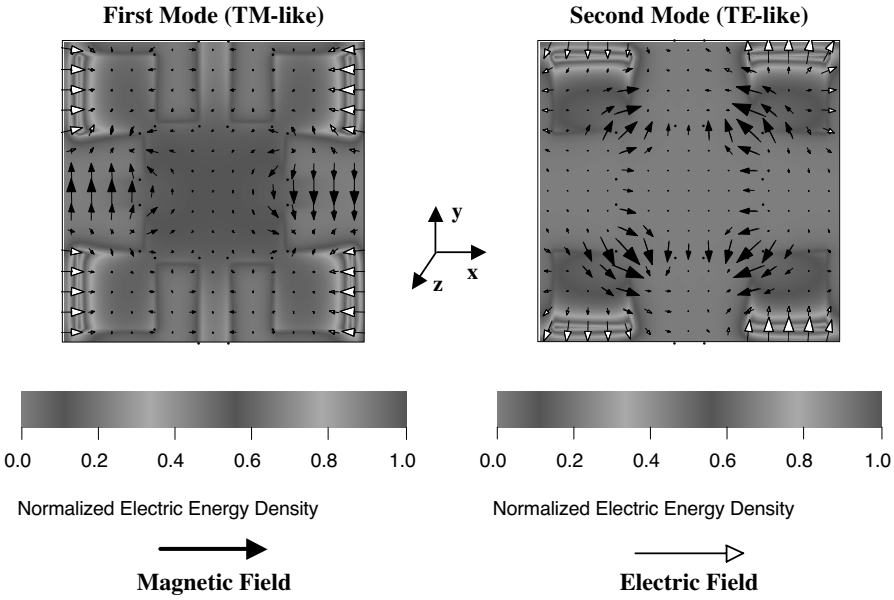

Figure 6. Electric field (white arrow), magnetic field (black arrow), and normalized electric energy density (gray) at a plane inside the dielectric substrate just underneath the metallic pattern.

impinged upon by an incident plane wave. Specifically, the magnitude of the reflection coefficient for both cases is equal to one, while the phase differs by 180. Alternatively, the conducting surface acts as an open circuit in the case of a PMC, and conversely as a short circuit in the case of a PEC. One way to present these short and open conditions is by using a periodic pattern. In this scenario, each element of the periodic pattern provides an equivalent L and C parallel connection, which changes the surface impedance. At frequencies where the periodic loading presents an open circuit condition, a magnetic surface is created.

To examine the feasibility of using the proposed UC-PBG structure as a PMC, two scattering structures are fabricated on RT/Duroid substrate with a dielectric constant of 10.2 and thickness of 0.635 mm. The reference scatterer to be used as a PEC is clad with intact copper without introducing any imperfections. The second scatterer is a conductor-backed UC-PBG structure as shown in Fig. 4(b). Fig. 7 shows the phase difference between the UC-PBG and PEC surfaces. It can be seen that a magnetic surface is successfully realized at around 14 GHz, where a 180 phase difference is observed at that frequency.

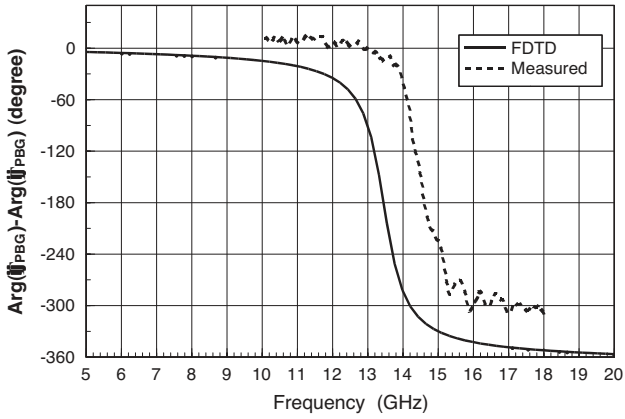

Figure 7. Measured and simulated phase difference between the conductor-backed UC-PBG and PEC surfaces.

Below 14 GHz, the surface is inductive; while above 14 GHz, it is capacitive. Good agreement is observed between the measured and simulated phase, with an error of around 6%.

3. APPLICATIONS

3.1. Spurious-Free Microstrip Filters

The broad stopband shown by the UC-PBG structure can be exploited to suppress spurious passbands always present in conventional microstrip filters [20–21]. The sharp cutoff, as shown in Fig. 3(b), can also be used to improve the roll-off of a lowpass filter (LPF). The integration of the UC-PBG structure with a conventional stepped-impedance lowpass filter was proposed in [21] to enhance its performance. The prototype, as shown in Fig. 8, shows stopband attenuation 38 dB better than that of a conventional LPF (Fig. 9). Integration of this UC-PBG lowpass filter with a drain mixer was presented in [21], where conversion gain enhancement and LO leakage reduction were demonstrated, as seen in Fig. 10.

3.2. Coupled Lines on UC-PBG Ground Plane

Parallel-coupled microstrip lines are widely used to design bandpass filters (BPF). Conventional BPFs, however, exhibits spurious passbands at harmonic frequencies, which may degrade overall system performance. This limitation can be overcome by designing the

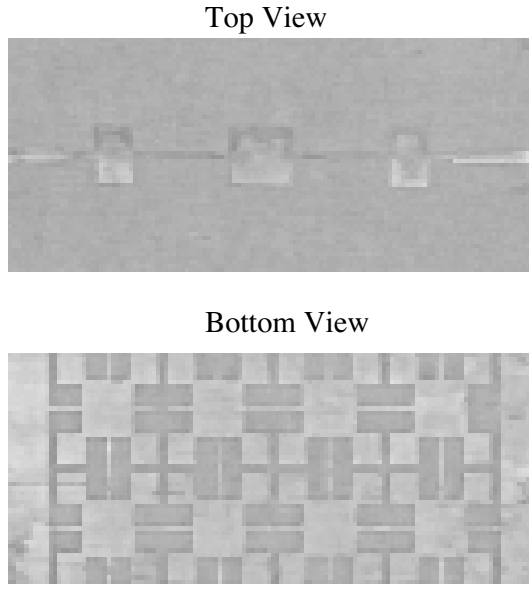

Figure 8. Photographs of top and bottom sides of the microstrip lowpass filter on the UC-PBG ground plane.

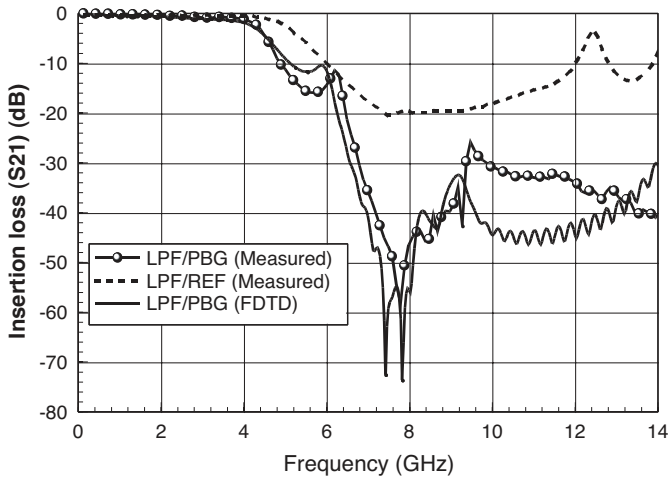

Figure 9. Measured and simulated insertion loss of the LPF on UC-PBG ground. S_{21} of a conventional LPF is also plotted for comparison.

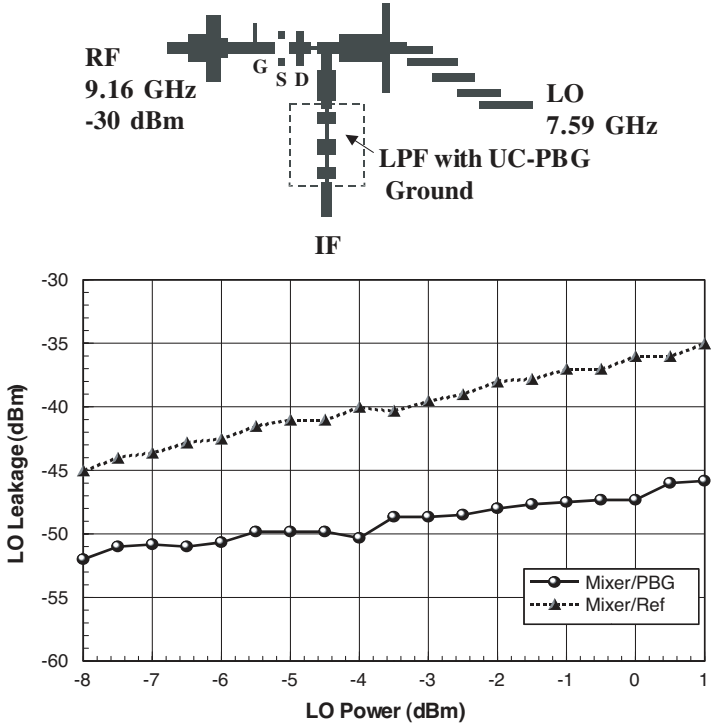

Figure 10. Leakage from LO port to IF port.

passband of the BPF inside the passband of the UC-PBG, while simultaneously placing the spurious passband of the BPF in the stopband [22]. In Fig. 11, a parallel-coupled BPF is built on the UC-PBG ground plane with a substrate thickness of 0.635 mm and a relative permittivity of 10.2. An analysis of the coupling effects of the coupled microstrip lines above the UC-PBG ground plane is necessary for proper BPF design [23].

Fig. 12 shows the characteristic impedance and effective dielectric constant of coupled-microstrip lines for various line widths and gap spacings. For a given configuration, both the even-mode impedance and effective dielectric constant are higher than those of the odd-mode case. As the ratio of the coupled-line gap (S) to substrate thickness (H) increases, the impedance and effective dielectric constant of the even and odd modes approach the same value. That is, they approach the impedance and effective dielectric constant values of a single microstrip line with the same width. Although the overall trend of variation is similar to that of coupled microstrip lines on a solid ground plane, a

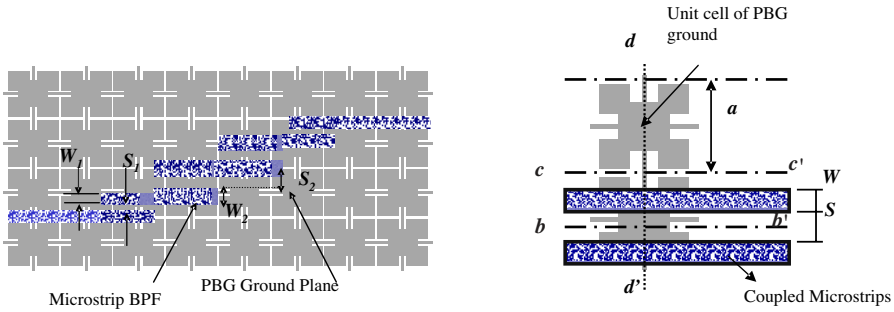

Figure 11. (a) Schematic of a parallel-coupled BPF on the UC-PBG ground plane, and (b) configuration of coupled microstrip lines on the UC-PBG ground plane.

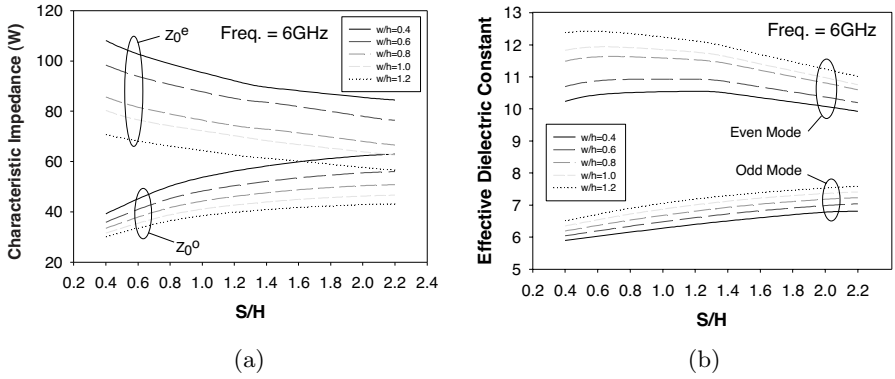

Figure 12. Calculated even- and odd-mode (a) characteristic impedance, and (b) effective dielectric constant.

significant increase of the even-mode impedance and effective dielectric constant has been observed. This phenomenon occurs because the slow wave effect generated by the UC-PBG ground plane strongly influences even-mode propagation. In contrast, the UC-PBG ground plane only weakly interacts with the odd-mode field distribution, so that both the odd-mode impedance and odd-mode effective dielectric constant for the UC-PBG coupled lines do not change significantly with respect to the solid ground plane case. Both the even-mode impedance and effective dielectric constant increase dramatically as the frequency approaches the first stopband, which starts at about 10 GHz [18].

Based on this analysis, a maximally flat bandpass filter with

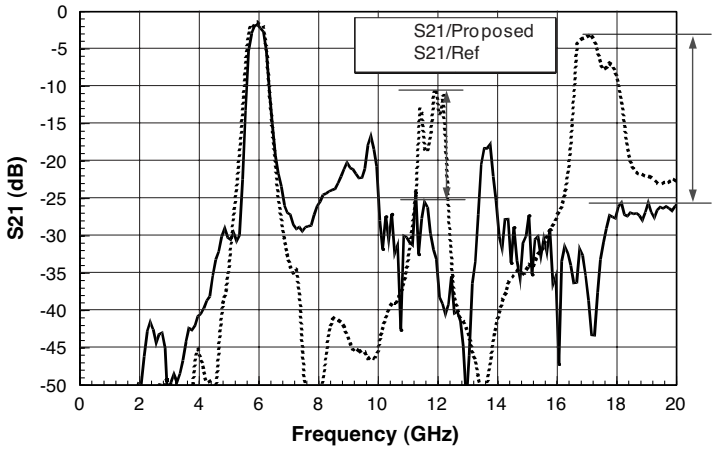

Figure 13. Measured insertion loss (S_{21}) of the BPF on UC-PBG ground. The insertion loss of a conventional BPF is also shown for comparison.

fractional bandwidth of 10% centered at 6 GHz has been designed for demonstration purpose. The filter consists of four sections of coupled microstrips on the periodically patterned ground plane. Prototype element values of a four-stage maximally flat response can be found from filter design tables [24]. These element values are then used to calculate the admittance inverter constants, J_n, by impedance scaling and frequency transformation. The even- and odd-mode characteristic impedance required to meet the filter specifications can be approximated by

$$Z_{0e} = Z_0[1 + JZ_0 + (JZ_0)^2], \tag{1}$$

$$Z_{0o} = Z_0[1 - JZ_0 + (JZ_0)^2], \tag{2}$$

where Z_0 is the characteristic impedance of the isolated microstrip on UC-PBG ground. Once the even- and odd-mode characteristic impedances have been determined, the required strip width (W) and gap spacing (S) of the coupled lines can be found from the data in Fig. 12(a). The resonator length can be roughly estimated using the even-mode effective dielectric constant shown in Fig. 12(b). Fig. 13 shows the measured results of the proposed filter compared to that of the conventional edge-coupled filter. As can be seen, the measured insertion loss (S_{21}) of a conventional bandpass filter is -10 dB and -3 dB at 12 GHz and 17 GHz, respectively. In contrast, the proposed UC-PBG filter exhibits 20 dB to 25 dB spurious rejection in the second

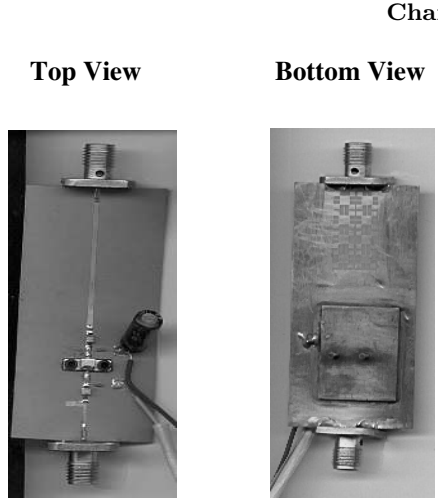

Figure 14. Photographs of the S-band class-AB power amplifier integrated with UC-PBG microstrip for harmonic tuning.

and third passband. This is in addition to the low insertion loss (1.6 dB) and narrow bandwidth (9%) recorded in the main passband. Moreover, the slow-wave effect reduces the resonator length of the filter integrated with the UC-PBG ground plane by 20% when compared to a conventional filter [23]. This sizable reduction is made possible because of the enlarged even-mode effect dielectric constant values presented by the UC-PBG lattice.

3.3. Harmonic Tuning in Power Amplifier

Power amplifier is the main power consumption block in any advanced wireless communications system. The most crucial factor in power amplifier design is to increase the power-added efficiency (PAE) and output power. It is possible to tune both the second and third harmonics in order to achieve higher PAE [25–26]. For example, harmonic tuning in power amplifier design using the UC-PBG structure was demonstrated in [27]. Fig. 14 shows the prototype of an S-band class AB power amplifier integrated with UC-PBG microstrip. The UC-PBG dimensions were designed to have a cut-off frequency at 6 GHz with a wide stopband from 6 to 15 GHz [27]. The output levels of the second and third harmonics have been reduced from −11 dB and −30 dB to −48 dB and −60 dB, respectively, as compared to a reference amplifier terminated with a standard 50-Ω load. A 10% increase in PAE and 1.3 dB increase in output power were also realized.

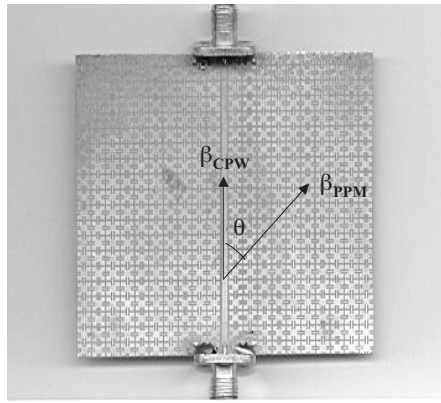

Figure 15. Photograph of the CB-CPW with UC-PBG structure in the lateral ground planes. Underneath the CPW is a backed conductor. Propagation directions of CPW and Parallel-plate modes are indicated.

3.4. Leakage Suppression in CB-CPW

Coplanar waveguide (CPW) has been studied extensively and applied both to MIC and MMIC [28] for its low dispersion characteristic. The conventional CPW is often backed with a ground plane to enhance mechanical strength or to provide heat sink capabilities [29]. However, the main drawback of the conductor-backed CPW (CB-CPW) is the power leakage due to the undesired parallel-plate mode. This leakage can be suppressed using shorting posts [30]. Although effective, this solution is costly and a planar structure is preferred to simplify the fabrication process. The stopband of the 2D UC-PBG structure on a grounded dielectric slab can be used to suppress the parallel-plate mode of the CB-CPW [31].

Fig. 15 shows the novel CB-CPW where the UC-PBG lattice is etched on the top ground planes and an additional ground plane is added to the backside. The measured transmission coefficient (S_{21}) of the proposed CB-CPW on UC-PBG substrate is shown in Fig. 16 in comparison to conventional CPW and CB-CPW. For conventional CB-CPW, the leakage is significant at all frequencies, as expected. The insertion loss of a conventional CPW is relatively low at frequencies below 13 GHz, and starts rippling at higher frequencies due to reflections caused by connectors. As can be seen from Fig. 16, power leakage from the CB-CPW with UC-PBG is still present in the range from DC to 9 GHz, which is the passband of the UC-PBG structure. However, the insertion loss is significantly improved between 9 GHz and 14 GHz. This phenomenon can be explained by considering the

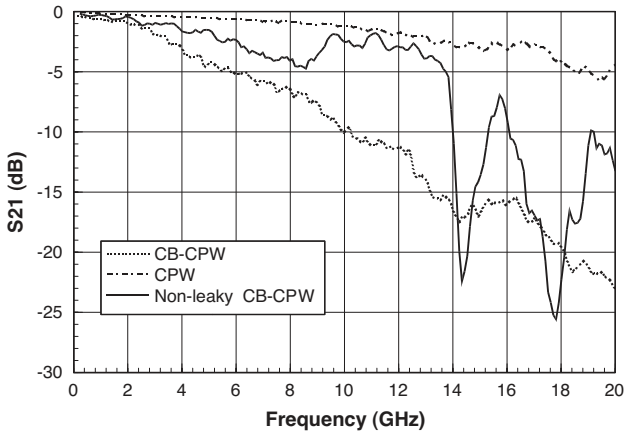

Figure 16. Measured insertion loss of the CB-CPW with lateral UC-PBG ground. S_{21} of conventional, non-leaky CPW and CB-CPW are also plotted for comparison.

propagation angle θ of the TEM parallel plate mode responsible for power leakage. When measured from the CPW axis, θ can be estimated as

$$\theta = \cos^{-1}\left(\frac{\beta_{\mathrm{CPW}}}{\beta_{\mathrm{PPM}}}\right), \tag{3}$$

where β_{CPW} and β_{PPM} are the propagation constant of the CPW and the parallel plate mode, respectively. In the case of the standard CB-CPW with dimensions given in [22] and [31], θ is about 36.5° degrees in the frequency range 9 to 14 GHz. In the case of CB-CPW with UC-PBG, β_{PPM} can be estimated using the computed dispersion diagram (Fig. 5(b)). The average effective dielectric constant of the first mode in the (X-M) section of the dispersion diagram, which describes propagation for angles from 0° to 45° with respect to the lattice primitive vectors, is 34.3°. Using this value, it is possible to estimate the propagation constant and thus the propagation angle θ of the parallel plate mode. Doing so for the CB-CPW line with UC-PBG reveals the angle θ varies from 64° to 65.7° for frequencies from 9 to 14 GHz. These values of θ correspond to directions of propagation for the parallel plate mode in the shadowed region of the dispersion diagram (Fig. 5(b)). The computed stopband for those directions of propagation is seen to be in the range 9.5 to 14.35 GHz, which agree well with measured data (Fig. 16).

3.5. Aperture Coupled Patch Antenna on UC-PBG Substrate

Microstrip patch antennas are extensively used in communication systems for their low profile, low cost and easy fabrication. Patch antennas are usually built on low permittivity substrates for optimum performance, since surface waves are usually excited on high dielectric constant substrate. On the other hand, MIC and MMIC are usually built on high dielectric constant substrates to reduce dimensions. In order to achieve a high degree of integration, it is desirable to realize patch antennas with good performance on high permittivity substrates. However, high permittivity substrates will invariably lead to narrower bandwidth. Although this problem can be alleviated by increasing the substrate thickness, the antenna efficiency is reduced because of surface-wave losses. The stopband provided by the UC-PBG structure can be employed to reduce surface-wave losses of patch antennas on high permittivity substrates [32–33]. Fig. 17 shows the top view of an aperture coupled patch antenna surrounded by three periods of the UC-PBG structure. The antenna has been designed to resonate at a frequency inside the UC-PBG stopband so that excitation of surface waves is reduced as much as possible. Details on the antenna and feeding structure geometry can be found in [33]. Fig. 18 shows the measured Co-polar E- and H-plane patterns of the UC-PBG antenna in comparison to a reference aperture-coupled patch antenna. It is seen that excitation of surface waves is strongly reduced in the E-plane and that directive gain at broadside of the UC-PBG antenna is 3 dB higher than that of the reference patch. The measurements were done at slightly different frequencies for the two antennas in order to have the same return loss ($S_{11} = -20$ dB) for both antennas. Cross-polarization level on both planes is below -10 dB. The asymmetry in the E-plane pattern is believed to be associated to the blocking effect of the connectors and coax cable used to connect the antenna under test to the spectrum analyzer. The ripples in E-plane pattern are due to the substrate edges. The null observed in the E-plane pattern at 315° is due to destructive interference caused by the four metallic screws used to joint the two-layer structure.

3.6. TEM Waveguide

Rectangular waveguides with uniform field distributions are of great concern for applications in quasi-optical power combining [34]. A TEM-waveguide can be realized by placing PMC on the two sidewalls of a waveguide, creating a magnetic boundary condition to suppress the parallel-plate mode. The UC-PBG structure has already been

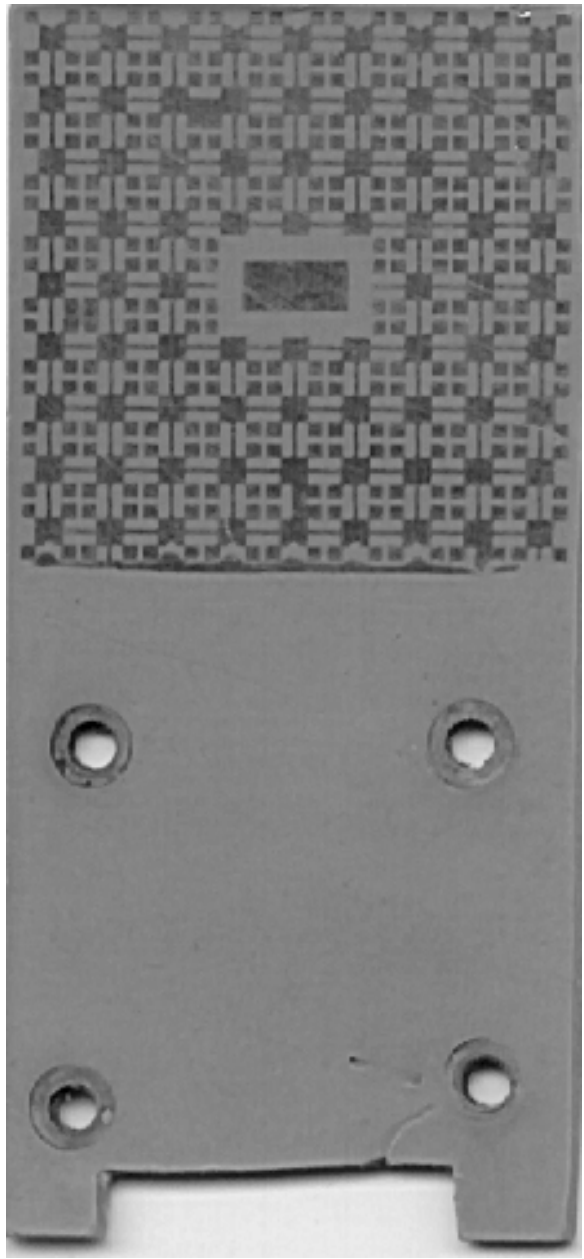

Figure 17. Top view of aperture coupled patch antenna surrounded by three periods of UC-PBG lattice.

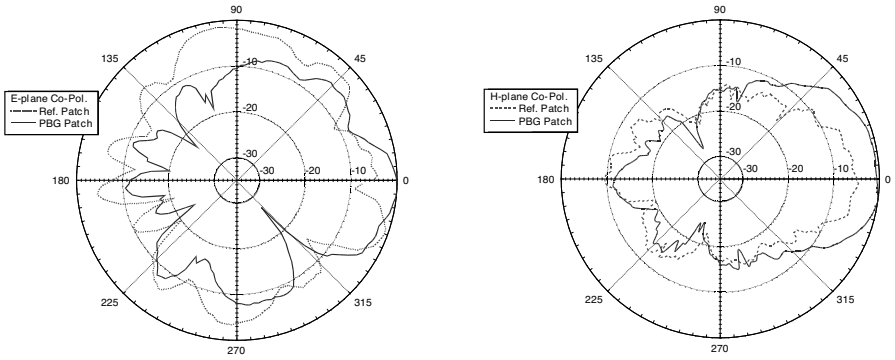

(a) (b)

Figure 18. Measured radiation patterns of reference and UC-PBG antenna. (a) *E*-plane, co-polar component. (b) *H*-plane, co-polar component.

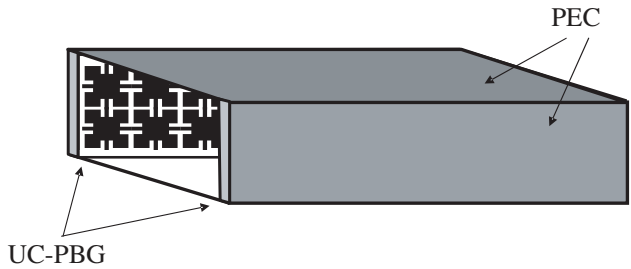

Figure 19. Schematic of the TEM-waveguide.

demonstrated to behave like a perfect magnetic conductor (PMC) within its stopband [35], and therefore can be applied to build a TEM-waveguide [36], as shown in Fig. 19.

In the proposed TEM waveguide, the measured phase velocity is 20% slower than that of a standard waveguide and reaches a minimum of 3.14×10^8 m/s at 9.8 GHz, as illustrated in Fig. 20(a). The velocity curve is relatively flat and close to the speed of light from 9 GHz to 10.2 GHz, indicating that a TEM mode has been created. Figure 20(b) illustrates the measured *E*-field strength of the proposed TEM waveguide at 10 GHz in comparison to a standard waveguide. For the standard waveguide,the *E*-field strength decreases from the maximum to zero as the observation point moves from the center to the conducting wall. On the other hand, the field distribution in the UC-PBG waveguide is more uniform and maintains 60% of its maximum

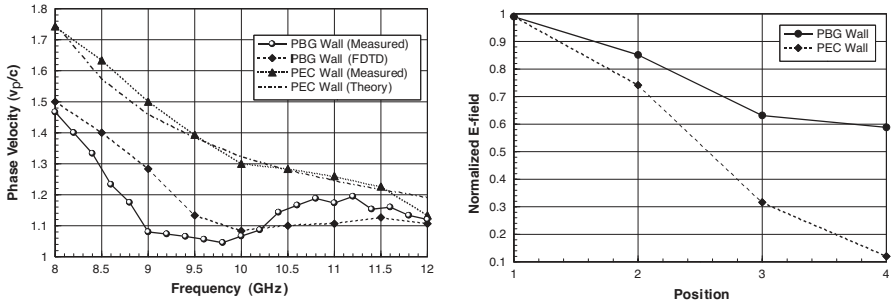

(a) (b)

Figure 20. Measured (a) phase velocity and (b) E-field strength of the TEM waveguide.

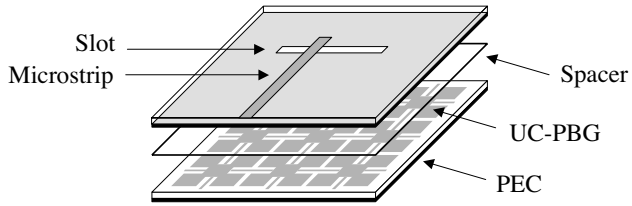

Figure 21. Schematic of CBS antenna using UC-PBG substrate.

value when probing near the side wall.

3.7. Cavity-Backed Slot Antenna Using UC-PBG Substrate

The cavity-backed slot (CBS) antenna is a suitable radiator element that finds applications in many different fields, e.g., high-gain phased arrays and mobile communications. The back cavity is used to prevent undesired backside radiation in order to generate a unidirectional radiation pattern. The cavity height, however, has to be an odd-multiple of quarter-wavelengths at the operating frequency in order to obtain good impedance matching [37]. Conceptually, the quarter-wavelength back conductor can be transformed to an open circuit in shunt with the slot. Therefore, a PMC can also be used to achieve the same effects while reducing the antenna volume substantially. We previously showed that the UC-PBG surface exhibits equivalent open-circuit characteristics at a certain frequency, and in turn can be used as a PMC at this frequency [35]. Fig. 21 shows the proposed low-profile cavity-backed slot antenna using the UC-PBG structure [38]. On the top is a microstrip line that acts as the feeding mechanism. A thin substrate is inserted between the slot antenna and the UC-PBG

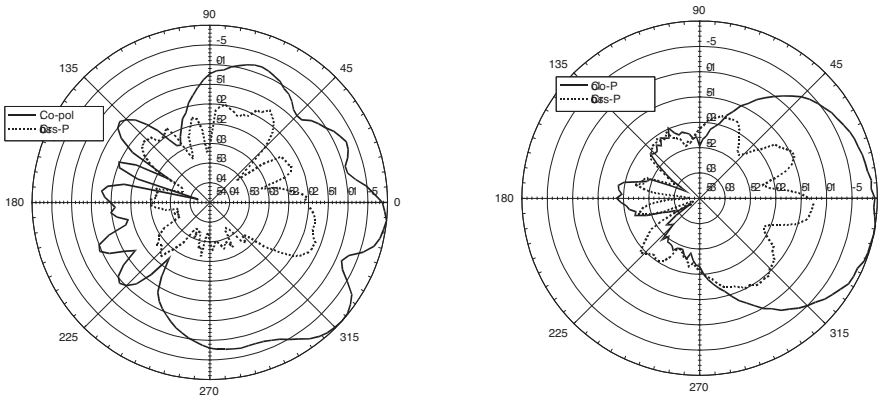

(a) (b)

Figure 22. Measured normalized (a) E-plane and (b) H-plane radiation patterns of the proposed CBS ant

in order to prevent direct shorting of the UC-PBG and the ground plane. The slot antenna is designed at 12.05 GHz with a 10 dB bandwidth of 5.8%. Fig. 22 shows the measured normalized E- and H-plane radiation patterns at 12.05 GHz. The front-to-back ratio is 15 dB for the E-plane and 18 dB for the H-plane patterns. The cross-polarization level is 12 dB to 15 dB below the co-polarization level for both planes. The cavity height of the proposed CBS antenna is much smaller (0.889 mm) than that of a conventional slot antenna backed by a quarter-wavelength (6.248 mm) metallic cavity.

4. CONCLUSION

Basic properties of UC-PBG structures and their applications to microwave circuits and antennas have been presented. The planar characteristic of UC-PBG structures makes them very attractive for applications to MICs and MMICs due to their excellent compatibility, ease of fabrication, and low cost.

The novel UC-PBG structure realizes a 2-D periodic LC network that increases the propagation constant of waves traveling along the structure itself. The dispersion diagrams of UC-PBG metallic pattern on both bare and conductor-backed dielectric slab have been calculated using FDTD, showing complete stopbands in different frequency ranges.

These unique features of the UC-PBG structure have been applied to different types of microwave circuits. Its broad stopband has been

exploited to suppress harmonics at the output of power amplifiers and to suppress spurious passbands of conventional microstrip filters. The slow-wave effect generated by the UC-PBG structure reduces resonator length in the construction of an edge-coupled bandpass filter. The realization of a PMC surface using conductor-backed UC-PBG allows the implementation of TEM waveguides and low-profile cavity-backed slot antennas. Other applications that have been demonstrated include reduction of parallel-plate mode leakage in CB-CPW and suppression of surface waves generated by patch antennas on high permittivity substrates.

ACKNOWLEDGMENT

This work was supported by the ARO Low Power, Low Noise MURI under contract DAAH04-96-1-0005.

REFERENCES

1. Yablonovitch, E., "Photonic band-gap structures," *J. Optical Soc. America B*, Vol. 10, 283–295, Feb. 1993.
2. Joannopoulos, J. D., R. D. Meade, and J. N. Winn, "Electromagnetic modeling for microwave imaging of cylindrical buried inhomogeneities," *Photonic Crystals*, Princeton Univ. Press, Princeton, NJ, 1995.
3. Sievenpiper, D. F., M. E. Sickmiller, and E. Yablonovitch, "3D wire mesh photonic crystals," *Phys. Rev. Lett.*, Vol. 76, 2480–2483, Apr. 1996.
4. Shumpert, J., T. Ellis, G. Rebeiz, and L. Katehi, "Microwave and millimeter wave propagation in photonic band-gap structures," *AP-S/URSI*, 678, 1997.
5. Qian, Y., V. Radisic, and T. Itoh, "Simulation and experiment of photonic band-gap structures for microstrip circuits," *Asia-Pacific Microwave Conf. (APMC'97) Dig.*, 585–588, Dec. 2–5, 1997.
6. Brown, E. R., C. D. Parker, and E. Yablonovitch, "Radiation properties of a planar antenna on a photonic-crystal substrate," *J. Optical Soc. America B*, Vol. 10, 404–407, Feb. 1993.
7. Sigalas, M. M., R. Biswas, and K. M. Ho, "Theoretical study of dipole antennas on photonic band-gap materials," *Microwave Opt. Technol. Lett.*, Vol. 13, 205–209, Nov. 1996.
8. Yang, H. Y. D., N. G. Alexopoulos, and E. Yablonovitch, "Photonic band-gap materials for high-gain printed circuit an-

tennas," *IEEE Trans. Antenna Propagat.*, Vol. 45, 185–187, Jan. 1997.

9. Meade, R. D., K. D. Brommer, A. M. Rappe, and J. D. Joannopoulos, "Photonic bound states in periodic dielectric materials," *Phys. Rev. B.*, Vol. 44, 13772–13774, Dec. 1991.
10. Gauthier, G. P., A. Courtay, and G. M. Rebeiz, "Microstrip antennas on synthesized low dielectric constant substrates," *IEEE Trans. Antennas and Propagation*, Vol. 45, No. 8, 1310–1314, Aug. 1997.
11. Smith, G. S., M. P. Kesler, and J. G. Maloney, "Dipole antennas used with all-dielectric, woodpile photonic-bandgap reflectors: gain, field patterns, and input impedance," *Microwave and Optical Technology Letters*, Vol. 21, No. 3, 191–196, May 1999.
12. Brown, E. R. and O. B. McMahon, "Large electromagnetic stop bands in metallodielectric photonic crystals," *Applied Physics Letters*, Vol. 67, No. 15, 2138–2140, Oct. 9, 1995.
13. Fan, S., P. R. Villeneuve, and J. D. Joannopoulos, "Large omnidirectional band gaps in metallodielectric photonic crystals," *Physical Review B (Condensed Matter)*, Vol. 54, No. 16, 11245–11251, Oct. 1996.
14. Sievenpiper, D., E. Yablonovitch, J. N. Winn, S. Fan, P. R. Villeneuve, and J. D. Joannopoulos, "3D metallo-dielectric photonic crystals with strong capacitive coupling between metallic islands," *Physical Review Letters*, Vol. 80, No. 13, 2829–2832, March 1998.
15. Sievenpiper, D. and E. Yablonovitch, "Eliminating surface currents with metallodielectric photonic crystals," *IEEE MTT-S Symp. Dig.*, 663–666, Baltimore, MD, June 7–12, 1998.
16. Qian, Y., D. Sievenpiper, V. Radisic, E. Yablonovitch, and T. Itoh, "A novel approach for gain and bandwidth enhancement of patch antennas," *IEEE RAWCON. Symp. Dig.*, 221–224, Colorado Springs, CO, Aug. 9–12, 1998.
17. Qian, Y., F. R. Yang, and T. Itoh, "Characteristics of microstrip lines on a uniplanar compact PBG ground plane," *Asia-Pacific Microwave Conf. (APMC'98) Dig.*, 589–592, Dec. 1998.
18. Yang, F. R., Y. Qian, R. Coccioli, and T. Itoh, "A novel low loss slow-wave microstrip structure," *IEEE Microwave Guided Wave Lett.*, Vol. 8, 372–374, Nov. 1998.
19. Kwon, Y. R., V. M. Hietala, and K. S. Champlin, "Quasi-TEM analysis of 'slow-wave' mode propagation on coplanar microstructure MIS transmission lines," *IEEE Trans. Microwave Theory*

Tech., Vol. MTT-35, 545–551, June 1987.

20. Yang, F. R., Y. Qian, and T. Itoh, "A novel compact microstrip bandpass filter with intrinsic spurious suppression," *Asia-Pacific Microwave Conf. (APMC'98) Dig.*, 593–596, Dec. 1998.
21. Yang, F. R., Y. Qian, and T. Itoh, "A novel uniplanar compact PBG structure for filter and mixer applications," *IEEE MTT-S Int. Microwave Conf.*, 919–922, Anaheim, CA, June 13–19, 1999.
22. Yang, F. R., K. P. Ma, Y. Qian, and T. Itoh, "A uniplanar compact photonic-bandgap (UC-PBG) structure and its applications for microwave circuits," *IEEE Trans. Microwave Theory Tech.*, Vol. 47, No. 8, 1509–1514, Aug. 1999.
23. Yang, F. R., R. Coccioli, Y. Qian, and T. Itoh, "Analysis and application of coupled microstrips on periodically patterned ground plane," *IEEE MTT-S Int'l Symp.*, Vol. 3, 1529–1532, Boston, MA, Jun. 2000.
24. Matthaei, G. L., L. Young, and E. M. T. Jones, *Microwave Filters, Impedance-Matching Networks, and Coupling Structures*, Artech House, 1980.
25. Lane, J. R., R. G. Freitag, H.-K. Hahn, J. E. Degenford, and M. Cohn, "High-efficiency 1-,2-, and 4-W class B FET power amplifiers," *IEEE Trans. Microwave Theory Tech.*, Vol. 34, 1318–1325, Dec. 1986.
26. Duvanaud, C., S. Dietsche, G. Pataut, and J. Obregon, "High-efficiency class F GaAs FET amplifier operating with very low bias voltage for use in mobile telephone at 1.75 GHz," *IEEE Microwave Guided Wave Lett.*, Vol. 3, 268–270, Aug. 1993.
27. Hang, C., V. Radisic, Y. Qian, and T. Itoh, "High efficiency power amplifier with novel PBG ground plane for harmonic tuning," *Microwave Symp. Dig.*, 807–810, Anaheim, CA, June 13–19, 1999.
28. Gupta, K. C., R. Garg, I. Bahl, and P. Bhartia, *Microstrip Lines and Slotlines*, Artech House, 1996.
29. Shigesawa, H., M. Tsuji, and A. A. Oliner, "Conductor-backed slot line and coplanar waveguide: dangers and full-wave analyses," *IEEE MTT-S Int. Microwave Symp. Dig.*, 199–202, New York, NY, May 25–27, 1988.
30. Yu, M., R. Vahldieck, and J. Huang, "Comparing coax launcher and wafer probe excitation for 10 mil conductor backed CPW with via holes and airbridges," *IEEE MTT-S Int. Microwave Symp. Dig.*, 705–708, Atlanta, GA, June 14–18, 1993.
31. Ma, K. P., F. R. Yang, Y. Qian, and T. Itoh, "Nonleaky conductor-backed CPW using a novel 2-D PBG lattice," *Asia-*

Pacific Microwave Conf. (APMC'98) Dig., 509–512, Dec. 1998.

32. Yang, F. R., R. Coccioli, Y. Qian, and T. Itoh, "PBG assisted gain enhancement of patch antennas on high-dielectric constant substrate," *IEEE AP-S International Symposium*, 1920–1923, Orlando, FL, June 1999.
33. Coccioli, R., F. R. Yang, K. P. Ma, and T. Itoh, "Aperture coupled patch antenna on UC-PBG substrate," *IEEE Trans. Microwave Theory Tech*, Vol. 47, No. 11, 2123–2130, Nov. 1999.
34. Hashemi-Yeganeh, S. and C. Birtcher, "Theoretical and experimental studies of cavity-backed slot antenna excited by a narrow strip," *IEEE Trans. Antennas and Propagat.*, Vol. 41, 236–241, Feb. 1993.
35. Ma, K. P., K. Hirose, F. R. Yang, Y. Qian, and T. Itoh, "Realization of magnetic conducting surface using novel photonic bandgap structure," *Electronic Lett.*, Vol. 34, No. 21, 2041–2042, Oct. 1998.
36. Yang, F. R., K. P. Ma, Y. Qian, and T. Itoh, "A novel TEM waveguide using uniplanar compact photonic-bandgap (UC-PBG) structure," *IEEE Trans. Microwave Theory Tech.*, Vol. 47, No. 11, 2092–2098, Nov. 1999.
37. Yoshimura, Y., "A microstripline slot antenna," *IEEE Trans. Microwave Theory Tech.*, MTT-20, 760–762, Nov. 1972.
38. Yang, F., Y. Qian, and T. Itoh, "Low-profile cavity-backed slot antenna using UC-PBG substrate," *IEEE AP-S Int'l Symp.*, Vol. 3, 1796–1799, Salt Lake City, UT, July 2000.